The Observation of Substructures in Crystals with the Electron Microscope

H. G. F. Wilsdorf

The Franklin Institute Laboratories
Philadelphia, Pennsylvania

The term "substructure" encompasses a variety of dislocation arrangements including the well defined sub-boundaries. Detailed aspects of substructures were covered in review articles by Hirsch (1), and Amelinckx and Dekeyser (2). As early as 1954, the electron microscope had been used for the study of dislocation boundaries by means of the replica technique (3) which will be outlined in this article. Later, this method was also applied to investigations of slip bands, pile-ups and interactions of glide dislocations with sub-boundaries (4-6). Since 1956, dislocations (7) and stacking faults (8) have been studied even more directly by a new technique called diffraction electron microscopy. Immediately after its discovery, this technique provided experimental proof for the many concepts of dislocation theory and later on was instrumental in providing new information on dislocation substructures. The two techniques will be discussed, and their applicability to the study of substructures will be critically reviewed.

Replica Technique

The use of the standard type electron microscope became of interest to metallurgists with the development of replica techniques in 1940 (9). Since that time numerous variations of this technique have been devised which have been reviewed in considerable detail in the literature (10).

The principle of the replica technique is to cover the metal surface which is to be investigated, with a film not thicker than, say, 500 Å, whereby the thickness of the film with respect to the normal of the surface has to be controlled. Fig. 1a indicates the production of a SiO replica (11) by vacuum evaporation. Subsequently, the film has to be separated by chemical means from the metal and then is "shadow-cast" (Fig. 1b). Since the contrast in electron images is usually due to an electron scattering mechanism depending on the thickness and mass of the specimen, the shadow-cast substance to be evaporated under an angle of, say, 30° onto the specimen ought to have a high atomic number. Now, the specimen is ready for examination in the electron microscope at magnifications from 2,000X to 60,000X. The surface area that can be screened at a time is 1 mm x 0.1 mm or about 2 mm in diameter, depending on the roughness of the surface, the microscope used, and other conditions.

Because of the inherent high resolving power of first class electron microscopes, details in the order of 25 Å can be detected. Obviously, this requires the careful preparation of metal surfaces, which, however, can be done with relative ease by applying suitable electropolishing procedures (12).

Turning to the subject matter of detecting sub-boundaries, it becomes clear that this technique permits their study at the line of intersection with the surface. For a tilt boundary with a $\theta = 5'$, the dislocations are separated by a

distance of about 2000 Å, which puts a rather stringent requirement on techniques that are used to mark the intercept of dislocations with the surface. Reference is made to the precipitation method and the etch pit technique. The former method was actually used to provide the first visible evidence of dislocations in a metal (3) and is based on the preferential nucleation of a precipitate at a dislocation site. Figs. 2a and b give examples of sub-boundaries which were found in the as-grown crystals of an Al-4% Cu alloy. Assuming that each precipitate marks the point of emergence of an edge dislocation, the misorientation between the two sub-grains can be calculated as $\theta = b/h$, where b is the Burgers vector and h the distance between the precipitates. The good agreement between measurements with the electron microscope and x-ray data (13) justifies the assumption that each dislocation gives rise to one precipitate.

Etch pit techniques have been successfully used to indicate the position of dislocations at surfaces, and many crystals have been thoroughly studied with this method using the light microscope (14). The limited resolving power of the light microscope led to the application of replica techniques and observations with the electron microscope. In particular, α-brass crystals have been studied extensively, and Figs. 3a and b demonstrate the ability of the technique (15-18). The points of emergence of dislocations are indicated by well defined etch pits which are small enough as to give a clear indication of the dislocations' arrangement. Fig. 3a shows a grown-in sub-boundary, and in Fig. 3b the interaction of glide dislocations with a sub-boundary can be seen.

The spatial distribution of sub-boundaries can be determined to some extent by repeatedly removing thin surface layers and replicating the same area with a suitable technique (19). It can be concluded that the replica method, in conjunction with precipitation and etch pit techniques, is capable of detecting the dislocation arrangements in sub-boundaries at their intersections with surfaces. Recent investigations by Young (20) and Levinstein and Robinson (21) with the light microscope indicate the possibility of applying the replica technique to etch pit studies in deformed pure f.c.c. metals which contain dislocation tangles.

Diffraction Contrast

The detection of lattice defects with the electron microscope is based on the diffraction of electrons by crystal lattices. The diffraction conditions have been given by von Laue in the fundamental equation

$$\underline{k}-\underline{k}_o = \underline{g} \cdot \lambda \qquad (1)$$

where $\underline{k}_o$ and $\underline{k}$ are the wave vectors of the incident and diffracted beam, λ the wavelength, and $\underline{g}$ a lattice vector in the reciprocal lattice which is equal to $g_1\, \underline{a}^* + g_2\, \underline{b}^* + g_3\, c^*$, g_1, g_2, g_3 being integers and a^*, b^*, c^* unit vectors in the reciprocal lattice. Fig. 4 represents the above relation in two dimensions in graphical form, and also shows the direction of the diffracted beam. According to Ewald's construction, diffraction occurs when a sphere with radius $1/\lambda$ and 0 as its center cuts through the intensity distribution of a reciprocal lattice point.

The amplitude of the diffracted wave can be written with the help of the structure factor F

$$A = |F| = \sum_n f_n \exp \left[2\pi i (\underline{k} - \underline{k}_o) \cdot \underline{r}_n\right] \tag{2}$$

where f_n is the scattering factor for electrons and the vector $\underline{r}_n$ marks the position of the scattering atom in a column of unit cell dimensions as measured from the origin of the lattice. However, if the Ewald sphere does not exactly pass through a reciprocal lattice point G but lies at a small distance from a given G as measured by the vector $\underline{s}$, then we have to replace $\underline{k} - \underline{k}_o$ by $\underline{g} + \underline{s}$. Since $\underline{g} \cdot \underline{r}_n$ is an integer, equation (2) becomes

$$A = f_n \sum_n \exp (2\pi i \underline{s} \cdot \underline{r}_n). \tag{3}$$

f_n has been taken out of the sum, which is permissible under the reasonable assumption that all the unit cells in the column are similar. So far, the case of a perfect crystal has been considered. Our main concern, however, is to show the formation of images of lattice defects. Following the calculations by Hirsch, Howie and Whelan (22) and in accordance with the nomenclature introduced by them, a deviation of the scattering atom from its ideal position will be defined by the vector $\underline{R}$. Now, the amplitude of the diffracted wave is obtained by adding a phase factor $\overline{\alpha} = 2\pi \underline{g} \cdot \underline{R}$ to equation (3), and α being a function of z (see Fig. 5) we can write

$$A \approx \int_{\text{column}} \exp (2\pi i \underline{g} \cdot \underline{R}) \cdot \exp (2\pi i s z) \, d z \tag{4}$$

s is now the distance between the Ewald sphere and G, taken in the direction of the column.

Equation (4) provides the foundation for discussing the formation of dislocation images in the electron microscope. First, we will consider the path of electron beams in the microscope. It follows from the principle of diffraction contrast that the diffracted beam (or beams) have to be prevented from contributing to the electron image. This is effected by an objective aperture which is in the order of 10^{-3} rad.; Fig. 6 shows the path of rays for the formation of the first electron image. The distorted lattice around a dislocation is indicated by a line in the specimen, while the missing electrons in the image can be seen as the "white" line in the figure.

Next, we have to determine the displacement vector $\underline{R}$ in equation (4). Choosing a simple case, $\underline{R}$ will be given for a screw dislocation lying parallel to the z-axis of an orthogonal coordinate system and parallel to the surface of the foil. One finds that $\underline{R}_x$ and $\underline{R}_y$ are zero and that

$$\underline{R}_z = \frac{b}{2\pi} \theta = \frac{b}{2\pi} \arctan \frac{y}{x}, \tag{5}$$

with $\underline{b}$ the Burgers vector of the dislocation. Inserting (5) into equation (4), a decision concerning the choice of a diffracting beam for producing an image of

the dislocation can be made immediately. The phase factor α contains a product of the reciprocal lattice vector $\underline{g}$ and the Burgers vector $\underline{b}$, which becomes zero if the family of diffracting lattice planes and $\underline{b}$ are parallel. It can, therefore, be concluded that the highest contrast may be expected when the diffracting lattice planes are perpendicular to the Burgers vector, and it would be most desirable to select a diffraction spectrum in accordance with this consideration.

From equation (4) the intensity profile of a dislocation can be obtained. Hirsch, Howie and Whelan have calculated the line width with the help of amplitude-phase diagrams (22). Recently, the values of the integral (4) have been calculated by Gevers for $\underline{g} \cdot \underline{b} = n = 1, 2, 3$ and 4 (23), and his main results for $n = 1$ and $n = 2$ are given in Fig. 7. Three features are in evidence: (i) The image of a dislocation is shifted from its true position by a distance approximately equal to its width; (ii) The width of an edge dislocation is twice that of a screw dislocation; (iii) The intensity profile of dislocations is steeper on that side which faces the center position of the dislocation.

The true position of a dislocation can be determined by changing $\underline{g}$, i.e., by choosing a different diffraction plane, or by reversing the sign of $\underline{s}$, which can be achieved by tilting the specimen around a suitable crystallographic direction (24). Fig. 8 demonstrates the shift of the dislocation image in the vicinity of an extinction contour, i.e., due to a change of sign of s.

As has been already mentioned above, the displacement vector has to have a perpendicular component with respect to the diffracting lattice planes if a dislocation image is to be obtained. On the other hand, the disappearance of the image when $\underline{g} \cdot \underline{b} = 0$ can be used to confirm the Burgers vector, which in many investigations can be presumed from experimental conditions. It is a requisite for a Burgers vector determination to have a goniometer stage for positioning of the crystal in the microscope. For a meaningful determination of the Burgers vector, one desires to have other dislocations in the specimen which have a Burgers vector different from the first set in order to ascertain that the critical diffraction condition is satisfied. A further check can be provided by employing the dark field technique. Here, the objective aperture in the back focal plane is adjusted so as to permit only the diffracted beam chosen above to form the dark field image, and, of course, those dislocations for which $\underline{g} \cdot \underline{b} = 0$ should not be seen.

The determination of the sign of s is necessary if one wishes to know the sense of the Burgers vector, since the above techniques yield only its direction. Crystals for these investigations have a thickness of more than 1000 Å and usually also show Kikuchi lines, which consist for each spectrum of a dark and a light line, parallel to each other, against the background of inelastically scattered electrons. For $\underline{s} = 0$ the Kikuchi lines go through the center of the reciprocal lattice point, but for a positive or negative $\underline{s}$ (see Fig. 4) the Kikuchi lines are displaced to the right or to the left of the reciprocal lattice point, respectively, The location of the dislocation's image for a given lattice position with respect to the incident beam is given in Fig. 9 for a dislocation loop. Slight rotations of the specimen and the additional observation of the actual diffraction pattern together with the electron micrograph enable the unambiguous determination of the direction and the sense of the Burgers vector.

Any discussion concerning diffraction contrast in electron micrographs must include the formation of fringes. Integration of equation (3) yields for

a thin crystal

$$A \sim \frac{\sin \pi ts}{\pi s} \qquad (6)$$

which shows immediately that the intensity of a diffracted beam depends on both the thickness t as well as on s. The first case is realized in crystals with varying thickness, and in particular, in wedge-shaped specimens (Fig. 10a); the second occurs when a thin film is bent and the Ewald sphere cuts the reciprocal lattice point at different distances. The resultant contrast pattern is called an "extinction contour", and an example of it is shown in Fig. 10b.

A two-dimensional lattice defect resulting from a "mistake" in the stacking of closest-packed planes in a crystal lattice is of considerable importance and can easily be detected with this technique. In the f.c.c. lattice, a mistake in the stacking of octahedral planes, for example ABCAB/ABC..., can be described as a displacement of the two parts of the crystal by a vector $R = a/6 \langle 112 \rangle$, a being a lattice translation. Fig. 11a shows the two parts of the crystal divided by the stacking fault AB. The amplitude of the diffracted wave is calculated by means of equation (4), adding to the term for the perfect crystal (above the line AB) a term that contains the displacement $a/6 \langle 112 \rangle$. The resultant phase angle, α, equals 0° or $\pm 120^o$, which leads to a set of light-dark fringes from A' to B with a spacing

$$D = t_o \cot \phi \qquad (7)$$

where t_o is the so-called extinction distance. t_o is related to the electrons' wavelength λ, the accelerating voltage U and the lattice potential V_g.

Similar fringes may be observed when twin and grain boundaries lie under an oblique angle in the specimen (Fig. 12).

The above discussion of the diffraction contrast was based on the kinematical theory of electron diffraction. The validity of this theory breaks down for s approaching zero, i.e., when the Laue conditions are fulfilled exactly. Then use must be made of the dynamical theory of electron diffraction which takes into account the interaction of electron waves with the wave field inside the crystal. The latter treatment provides quantitative results for many of the problems discussed above. According to the dynamical theory (25), the fringe distance for stacking faults is half of that obtained for $\underline{s} > 0$ (see Fig. 11b), which is an important result concerning the possibility of distinguishing between stacking faults and grain boundaries and other diffraction fringes. So far only dislocations lying parallel to the plane of the foils have been considered. While their image showed uniform contrast, dislocations inclined against the surface of the foil have a dotted appearance (Fig. 12) which has been explained by the dynamical theory as intensity oscillations.

Reliability of Results Obtained by Diffraction Electron Microscopy

The high scattering power of matter for electrons demands the preparation of specimens for diffraction electron microscopy in the thickness range of a few thousand Angstroms. Usually this is done by electropolishing (12), and techniques for electromachining electron transparent crystal wafers from bulk specimens have been described in the literature (26).

Because of the reduction of thick metal crystals to very thin foils, one immediately raises the question of how representative the observed dislocation patterns really are. In a recent paper Ham claims that 60% of the dislocations in a rolled aluminum-silver alloy are lost in the preparation of the thin specimens (27). This conclusion is based on comparisons between dislocation densities of unaged and aged Al-0.5% Ag alloys which had been deformed by rolling 18% or 45%. Because of the formation of small silver aggregates in the aged alloy, it can be assumed that the free motion of dislocations is reduced. Since the aged specimens contained more than 2 times as many dislocations than the unaged specimens, Ham argues that at least 60% of dislocations in Al-0.5% Ag and, by inference in Al, are lost during the preparation of the thin specimen. If this result be correct, one would have to conclude that dislocation rearrangements during electropolishing would take place to an extent that the patterns observed in the microscope would not bear much resemblance to the dislocation arrangement in the bulk specimen.

The change of dislocation patterns in deformed aluminum single crystals has been investigated with the diffraction electron microscopy method, selecting specimen thickness as the variable (28). Indeed, a considerable loss of dislocations and their rearrangement was clearly measurable below a thickness of 1500 Å. However, it was found that the dislocation patterns did not change noticeably in foils from 2000 Å up to 8000 Å, the latter specimen thickness being the largest which permitted discernible dislocation contrast to be obtained at an acceleration voltage of 100 KV. It has been pointed out (28) that "image forces" will tend to pull dislocations out of the specimen, if they are parallel or almost parallel to the surface, and provided that the slip plane is sufficiently inclined against the foil's surface, which should not be covered with an elastically harder layer. The other major influence on dislocations is due to their tendency to reduce their line energy. This can be achieved by dislocations moving perpendicular to the surface while remaining in their slip planes. Clearly, the above considerations will be influenced by the frictional forces the dislocations have to overcome, which will vary greatly from metal to metal.

Before we return to the problem of measuring dislocation densities by the thin film technique, some experimental findings will be discussed which are related to the mobility of dislocations near the surface of a thin foil. Under certain experimental conditions, dislocations form patterns that are repeated throughout the specimen. As a first example, I am referring to square-shaped loops in Al-0.5% Mg which are obtained after annealing quenched specimens. In Fig. 13 a number of these loops are shown. The plane of the loops is only slightly inclined to the surface, which in one instance cuts through the loop (see arrow in Fig. 13). Although the shape of the loop has not been changed markedly, a short dislocation is seen to connect one end of the cut-off loop with the surface. Undoubtedly, this part of the dislocation has been moved out of the original plane of the loop by the driving forces discussed in the previous paragraph. However, no further changes seem to have taken place. A second example can be provided with the help of Fig. 14 which shows dislocation loops in a deformed molybdenum single crystal. Loops of this type are prismatic and apparently have been "punched out" by stress concentrations due to precipitates in the matrix. They number from five to approximately twenty and are mostly of similar diameter, which decreases somewhat with increasing distance from its origin. Again, the surface has cut through most of the loops without affecting their shape to a major degree.

One might also refer at this point to the numerous investigations carried out on many pure metals and alloys which have yielded much information as to the different dislocation behavior in these materials. From the above discussion it is concluded that, provided certain precautions are observed, the technique provides reliable information on dislocation arrangements in crystals.

Since the knowledge of dislocation densities in deformed crystals is of utmost importance to the understanding of the flow characteristics, the measurement of this quantity deserves to be given special attention. Most specimens for diffraction electron microscopy are prepared from large single crystals or test specimens by electrolytic cutting and polishing. In general, the final film has a thickness of a few thousand Angstroms and contains in an area of, say, $10\mu^2$, a number of macroscopic wrinkles. Although the angular deviation between adjacent areas may only be in the order of one minute of arc, it is sufficient to upset the diffraction condition. This in turn does not permit the observer to see dislocations in a large area without continuously adjusting the orientation of the specimen against the incident beam. Also, the diffracting lattice planes may contain the direction of the Burgers vector of one set of dislocations which would lead to too small a dislocation count. Again, tilting the specimen could correct this possible error in measurement.

In case the inherent difficulties of the technique have been overcome, the success of a dislocation count will also depend on the particular arrangement of these defects. Since the majority of dislocations will not be straight but kinked and curved, the actual measurement of dislocation lines per ccm is difficult. Moreover, this measurement requires the knowledge of the thickness of the specimen, the dislocation's glide plane and the angle of this glide plane to the foil's surface; often the experimental determination of the Burgers vector is needed. In principle, all of these measurements can be performed, but the process is cumbersome and time consuming. Only few instances are known where glide dislocations are distributed uniformly throughout the crystal, which is the main assumption for the discussion so far.

The agglomeration of dislocations into tangles or "diffuse" cell walls during plastic flow is more frequent. Here, the density of dislocations may become so high that cell walls or tangles appear as dark areas in the micrographs, which condition will not allow a dislocation count at all, or only over smaller areas. Of course, thinning the foil to 1000 Å or possibly less would enable the detection of single dislocations; however, this appears not to be possible without losing many of them to the surface and/or from their ararrangement. This is exactly what seems to have happened in the foils studied by Ham (27). His paper contains three electron micrographs which exhibit cell walls containing glide dislocations in (i) pure aluminum, (ii) unaged Al-0.5% Ag, and (iii) aged Al-0.5 Ag. While the latter micrograph shows dislocations not only in the cell walls but also in the areas between walls, the volume between cell walls in the first two micrographs is empty. It is known from other investigations (29) that aluminum contains small prismatic loops near glide dislocations. The absence of prismatic loops and some odd dislocations within the cells indicate that the final foils were too thin to permit reliable dislocation counts, while thicker foils would have obscured single dislocations in the cell walls. It stands to reason that diffraction electron microscopy is a suitable technique for dislocation counts in lightly deformed crystals with reasonably uniform dislocation density. However, for heavily deformed crystals the error of measurement is quite considerable, and Ham's data

on Al-0.5% Ag are not acceptable until the measurements have been repeated with single crystals which permit the counts in known crystallographic planes and an accurate determination of the specimen's thickness.

Summary of Applications

Many applications of the techniques discussed above to the numerous problems of substructures in crystals have been reported (30). It has been pointed out in the previous paragraph that diffraction electron microscopy is particularly useful for accurate measurements in the range of a few microns and less. This is the reason why the most significant results have been obtained on substructures in deformed metals, characterizing their role in yielding phenomena, plastic flow, by translation as well as twinning, and fracture. Since this method offers the highest resolution of all known experimental techniques for the study of dislocations, even sub-boundaries with spacings of less than 500 Å can be analyzed in great detail, provided the arrangement is fairly regular. This applies to all tilt and twist boundaries, and the investigation of recovery and recrystallization processes with this method can be very useful. Recently, the formation of dislocation networks in crystals with layer structures has received considerable attention. Since these crystals cleave easily parallel to their basal planes, specimen preparation is thus facilitated and, of course, it is of great advantage that the dislocations are lying parallel to the plane of the specimen. Usually, diffraction conditions are satisfied for areas larger than the field of view, and very beautiful micrographs have been taken from graphite, mica, talc, the bismuth-tellurides and others (31).

Certain substructures found in crystals grown by solidification methods have spacings in the order of 1 mm, and electron microscopy is not likely to contribute much to their explanation. The chances of coming across grown-in sub-boundaries in a thin film are rather small, and x-ray and etch pit techniques are more suitable for their study. However, in the field of epitaxial overgrowth diffraction microscopy could play an important role. According to Frank and van der Merwe (32), the misfit between two different lattices can be described in terms of interfacial dislocations, and interesting observations on PbS and PbSe and chromium bromide have recently been reported in the literature (33, 34).

The most interesting observations of substructures have been made on deformed crystals, and we will limit ourselves to a brief discussion of dislocation patterns in metal crystals. The state of the art until 1959 was summarized by Hirsch in a review article (35). In agreement with earlier surface studies on deformed metals (36), it was found that α-brass and the pure fcc metals respectively show different dislocation structures indeed. In α=brass and stainless steel (37) pile-ups were observed while in gold, copper and nickel the dislocations are arranged "in very complex three-dimensional networks at low deformation, and in poorly developed sub-boundaries at higher deformations." (35) Experimental evidence to this effect due to Tomlinson and Partridge was given in the above-mentioned review article by Hirsch (35) and by Whelan (38). These results were explained by considering dislocation interactions.

In 1959, Wilsdorf and Kuhlmann-Wilsdorf (29) pointed out that small prismatic dislocation loops were present near the irregularly arranged glide dislocations in lightly deformed aluminum and nickel. For several reasons, including the observation that the nature of these loops is the same as that of quenched-in loops (39-41), it was concluded that point defect interactions with

glide dislocations are responsible for the formation of the irregular and kinked dislocations in fcc pure metals. Along an individual dislocation line many curvatures of very small radii can be observed which are too small to be in equilibrium with the applied stress; i.e., dislocation lines are lying not in one slip plane but contain many super jogs. The fact that tangles occur at a glide strain of 0.05 in crystals oriented for single glide is strong proof that the responsible mechanism is based on point defect interactions and not on "forest cutting" (42-44).

Another unexpected dislocation phenomenon, discovered with the help of diffraction electron microscopy, is the presence of long, narrow dislocation loops which form behind screw dislocations parallel to $\langle 112 \rangle$. They were seen in aluminum (45), magnesium oxide (46), in zinc (47), copper (48,49,50), and in fatigued metals (48). In particular, the presence of these dislocation "dipoles" is most frequent in stage I of the stress-strain curve of f.c.c. crystals deformed at low temperatures (43,49,50). The reason that they are not seen at higher deformations under conditions of multiple slip or at elevated temperatures presumably is two fold: (i) intersecting dislocations will break up the dipoles; (ii) as shown by Price (47), the dipoles disintegrate into sequences of prismatic loops at temperatures which permit conservative climb.

Electron diffraction microscopy is the only technique which enables one to see the movement of dislocations. Hirsch, Horne, and Whelan (7) were the first to observe moving dislocations in aluminum foils. In these experiments an increase in intensity of the illuminating electron beam was used to induce the stresses which moved the dislocations. Soon afterwards, small straining devices were built for the deformation of thin foils in the electron microscope (51,52,53). This technique made possible the direct observation of dislocation propagation, their interactions with each other and with obstacles, cross-slip, pile-ups, dislocation sources and fracture (54,55,56). Later experiments made use of ribbons grown by vapor techniques and showed the formation of prismatic loops in the wake of glide dislocation. Information on climb was obtained by following the motion of R-dislocations (39) during the annealing of thin quenched aluminum foils in the microscope (57). Even the formation of precipitates in an aluminum-copper alloy and their dissolution at will by controlling the temperature cycle was possible (58).

Acknowledgement

I wish to thank my wife, Professor Doris Wilsdorf, University of Pennsylvania, Philadelphia, for valuable discussions.

The partial financial support by the Aeronautical Research Laboratory, Office of Aerospace Research, USAF, under Contract No. AF 33(616)-6996 is gratefully acknowledged.

References

1. Hirsch, P. B., Progress in Metal Physics 6, 236 (1956).

2. Amelinckx, S. and Dekeyser, W., Solid State Physics 8, 327 (1959).

3. Wilsdorf, H. and Kuhlmann-Wilsdorf, D., Phil. Mag. 45, 1096 (1954).

4. Wilsdorf, H. and Kuhlmann-Wilsdorf, D., Report of Conference on Defects in Cryst. Solids (London, Phys. Soc.), 1955, pp. 175.

5. Thomas, G. and Nutting, J., Institute of Metals Symposium on "Mechanism of Phase Transf. in Metals" (London), 1955, pp. 57.

6. Takeyama, T. and Koda, S. Nature (London) 179, 777 (1957).

7. Hirsch, P. B., Horne, R. W., and Whelan, M. J., Phil. Mag. 1, 677 (1956).

8. Bollmann, W., Phys. Rev. 103, 1588 (1956).

9. Mahl, H., Z. techn. Phys. 21, 17 (1940).

10. Muller, H., Praparation von Technisch-Physikalischen Objekten fur die Elektronenmikroskopische Untersuchung. Akad. Verlagsges., Leipzig, 1962.

11. Wilsdorf, H., Z. Metallkd. 45, 14 (1954).

12. Jacquet, P.A., Met. Reviews 1, 156 (1956).

13. Guinier, A., Imperfections in Nearly Perfect Crystals, Wiley 1952, p. 402.

14. Johnston, W. G., Progress in Ceramic Science 2, 1 (1961).

15. Sun, R. and Wilsdorf, H. G. F., J. Franklin Inst. 265, 413 (1958).

16. Wilsdorf, H. G. F., Internal Stresses and Fatigue in Metals, Elsevier, 1959, pp. 178.

17. Meakin, J. D. and Wilsdorf, H. G. F., Trans. AIME 218, 737 (1960).

18. Meakin, J. D. and Wilsdorf, Trans. AIME 218, 745 (1960).

19. Fourie, J. T., J. Appl. Phys. 29, 608 (1958).

20. Young, F. W., J. Appl. Phys. 33, 3553 (1962).

21. Levinstein, H. J. and Robinson, W. H., J. Appl. Phys. 33, 3149 (1962).

22. Hirsch, P. B., Howie, A., and Whelan, M. J., Phil. Trans. A 252, 499 (1960)

23. Gevers, R., Phil. Mag. 7, 59 (1962).

24. Howie, A. and Whelan, M. J., Proc. Roy. Soc. A 267, 206 (1962).

25. Whelan, M. J. and Hirsch, P. B., Phil. Mag. 2, 1121 (1957).

26. Strutt, P. R., Rev. Sci. Instr. 32, 411 (1961).

27. Ham, R. K., Phil. Mag. 7, 1177 (1962).

28. Wilsdorf, H. G. F. and Schmitz, J., J. Appl. Phys. 33, 1750 (1962).

29. Wilsdorf, H. G. F. and Kuhlmann-Wilsdorf, D., Phys. Rev. Letters 3, 170 (1959).

30. Thomas, G., Transmission Electron Microscopy of Metals, Wiley, 1961.

31. Amelinckx, S. and Delavignette, P., Direct Observations of Imperfections in Crystals, AIME, 1961, pp. 295.

32. Frank, F. C and van der Merwe, J. H., Proc. Roy. Soc. A 198, 205 (1959); Ibid. 200, 125 (1950); Ibid. 201, 261 (1950).

33. Matthews, J. W., Phil. Mag. 6, 1347 (1961).

34. Delavignette, P., Tournier, J., and Amelinckx, S., Phil. Mag. 6, 1419 (1961).

35. Hirsch, P. B., Met. Reviews 4, 101 (1959).

36. Kuhlmann-Wilsdorf, D. and Wilsdorf, H. G. F., Acta Met. 1, 394 (1953).

37. Whelan, M. J., Hirsch, P. B., Horne, R. W., and Bollmann, W., Proc. Roy. Soc. A 240, 524 (1957).

38. Whelan, M. J., Proc. Roy. Soc. A 249, 114 (1958).

39. Kuhlmann-Wilsdorf, D., Phil. Mag. 3, 125 (1958).

40. Hirsch, P. B., Silcox, J., Smallman, R. E., and Westmacott, K. H., Phil. Mag. 3, 897 (1958).

41. Kuhlmann-Wilsdorf, D. and Wilsdorf, H. G. F., J. Appl. Phys. 31, 516 (1960).

42. Kuhlmann-Wilsdorf, D., Maddin, R., and Wilsdorf, H. G. F., "Strengthening Mechanisms in Solids", ASM, 1962, pp. 175.

43. Kuhlmann-Wilsdorf, D. and Wilsdorf, H. G. F., Symposium on Electron Microscopy, Wiley, 1963.

44. Wilsdorf, H. G. F. and Schmitz, J., J. Appl. Phys. 33, 1750 (1962).

45. Fourie, J. T. and Wilsdorf, H. G. F., J. Appl. Phys. 31, 2219 (1960).

46. Washburn, J., Graves, G. W., Kelly, A., and Williamson, G. K., Phil. Mag. 5, 991 (1960).

47. Price, P. B., Phil. Mag. 5, 873 (1960).

48. Quoted by Hirsch, P. B. and Warrington, D. H., Phil. Mag. 6, 735 (1961).

49. Fourie, J. T. and Murphy, R. J., Phil. Mag. 7, 1617 (1962).

50. Basinski, Z. S., Proc. 5th Int. Congress Electron Microscopy, Academic Press 1962, B-13.

51. Wilsdorf, H. G. F., Rev. Sci. Instr. 29, 323 (1958).

52. Berghezan, A. and Fourdeux, A., Fourth Int. Conf. on Electron Microscopy, 567, Springer, 1960.

53. Kear, B. H., Rev. Sci. Instr. 31, 1007 (1960).

54. Wilsdorf, H. G. F., ASTM Special Technical Publication No. 245, 43 (1958).

55. Berghezan, A. and Fourdeux, J. Appl. Phys. 30, 1913 (1959).

56. Wilsdorf, H. G. F., Proc. Int. Conf. on Structure and Prop. of Thin Films, John Wiley, 1959, pp. 151.

57. Silcox, J. and Whelan, M. J., Proc. Int. Conf. on Structure and Prop. of Thin Films, John Wiley, 1959, pp. 164.

58. Thomas, G. and Whelan, M. J., Phil. Mag. 6, 1103 (1961).

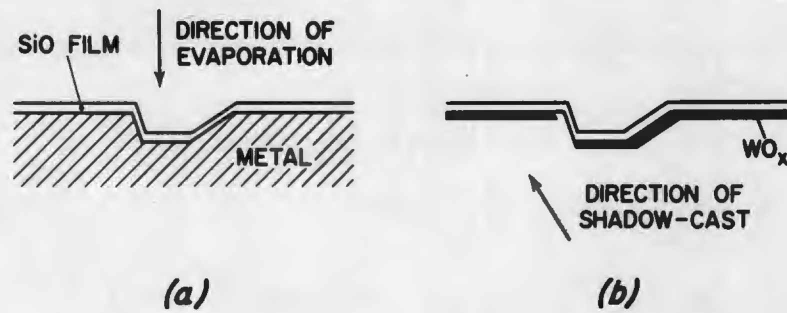

Fig. 1 Schematic representation of the preparation of a so-called "direct" replica. For details of the SiO replica technique, see reference (11).

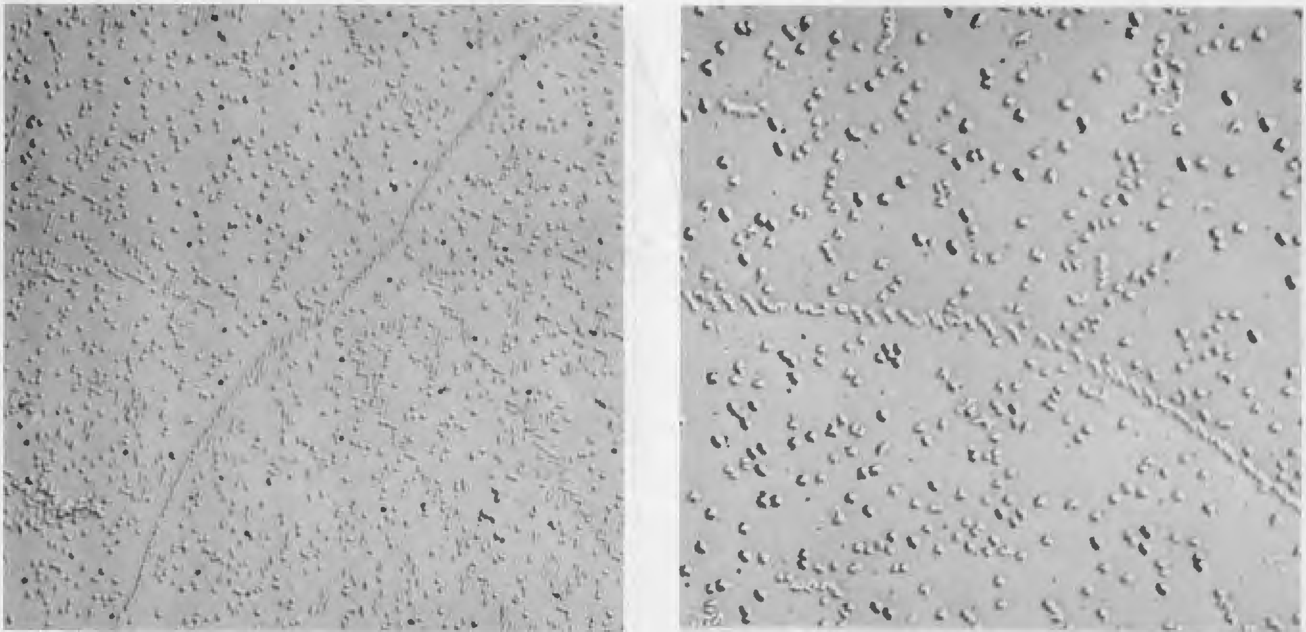

Fig. 2 Detection of the emergence of dislocations at the surface by a combined precipitation and replica technique.
(a) 9000:1; (b) 18000:1

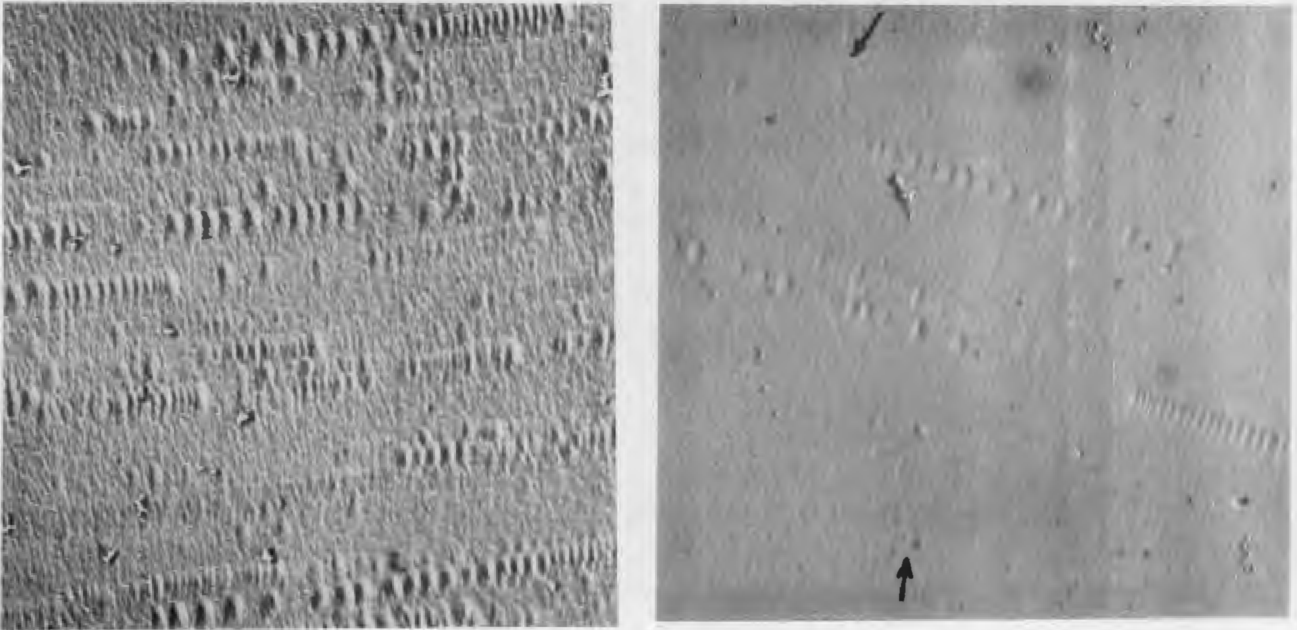

Fig. 3 Etch pits marking the sites of dislocations in deformed α-brass (Meakin and Wilsdorf (17,18)).
(a) 20000:1; (b) 15000:1 (arrows indicate sub-boundary)

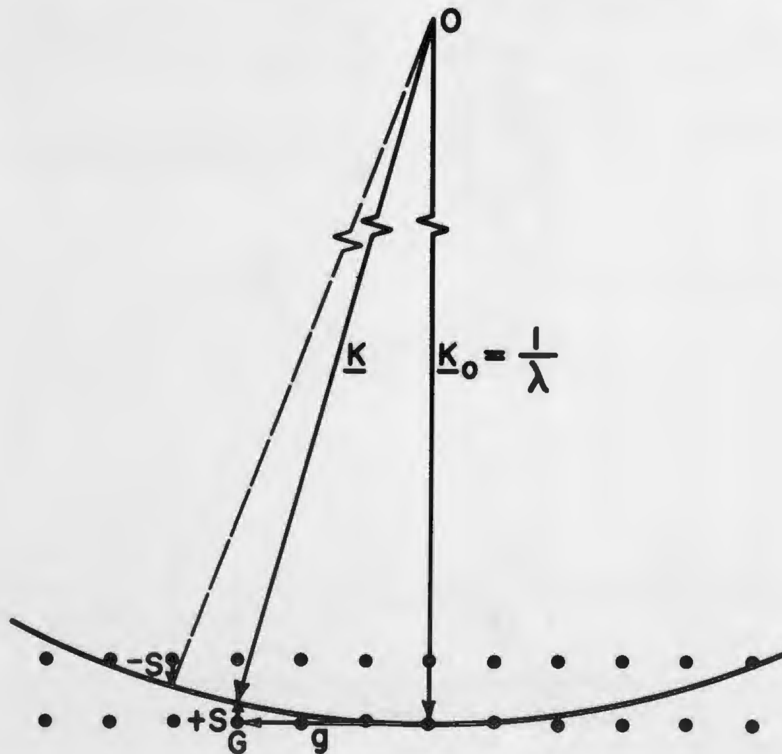

Fig. 4 Ewald's construction of the conditions for the diffraction of electrons in crystals. For explanation of symbols, see text.

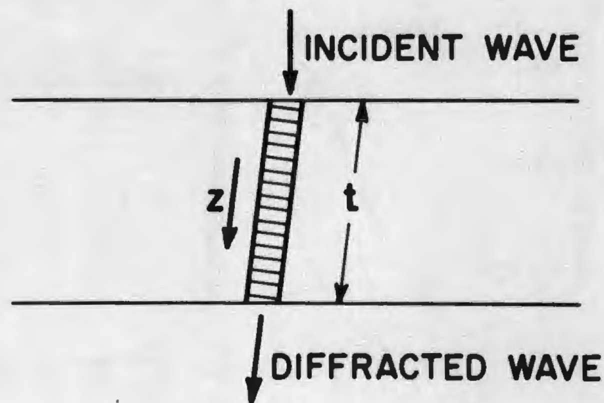

Fig. 5 Column in crystal used for the calculation of diffraction contrast.

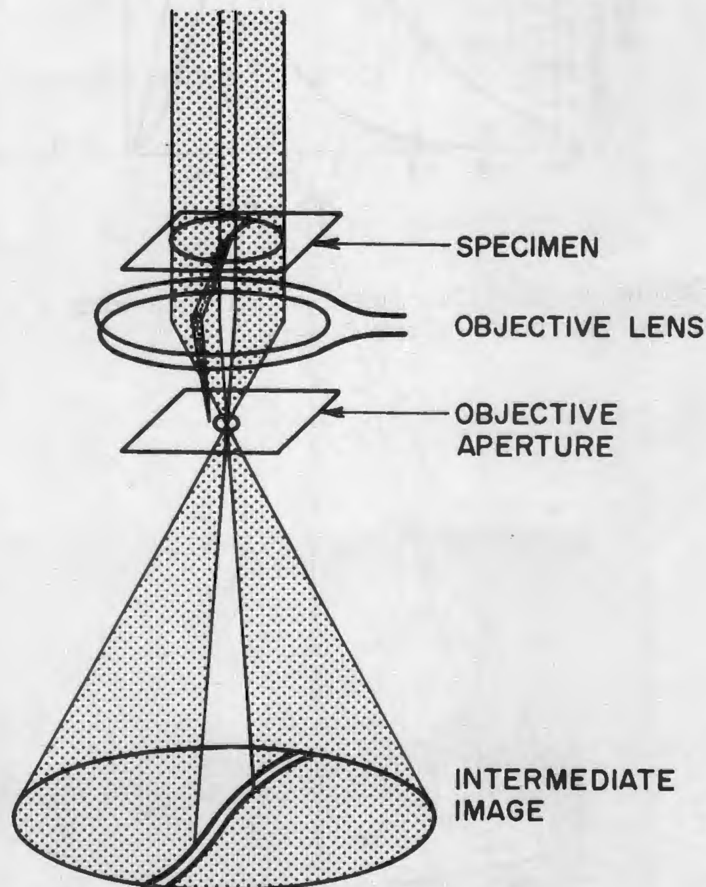

Fig. 6 Path of electrons passing through the specimen, or being diffracted into an angle larger than the objective aperture, forming the intermediate image. Dislocation is indicated as dark line in specimen.

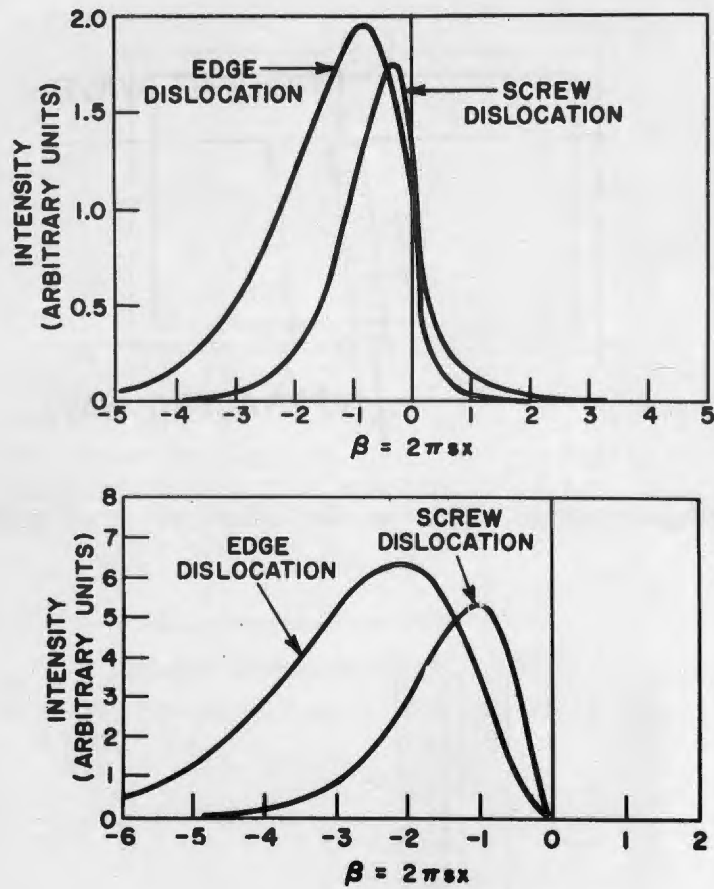

Fig. 7 Intensity profiles for dislocations with n = 1 (top) and n = 2 (bottom) (after Gevers (24)).

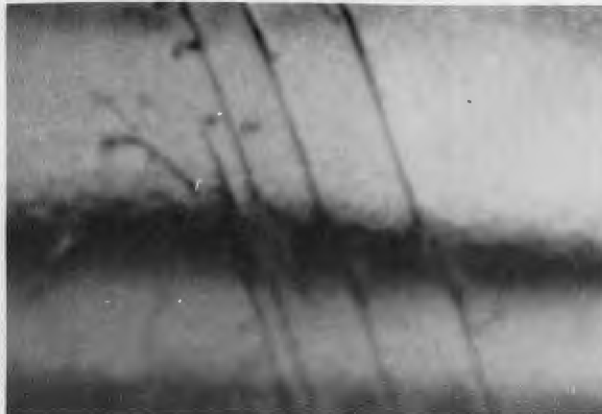

Fig. 8 Shift of the image of dislocations due to a change of s. 40000:1

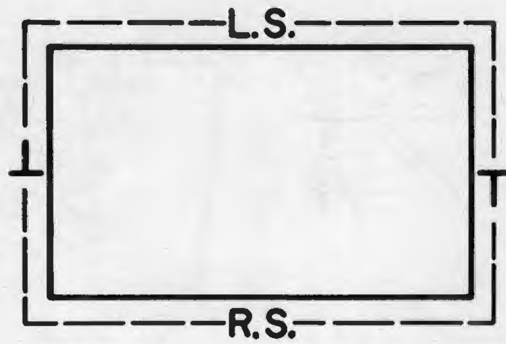

Fig. 9 Sketch illustrating that the image of a dislocation loop is lying either "inside" or "outside" of the true location of the dislocation loop. L.S. and R.S. indicate left and right-handed screw dislocation respectively.

Fig. 10a Diffraction fringes due to changing thickness of specimen. 13000:1

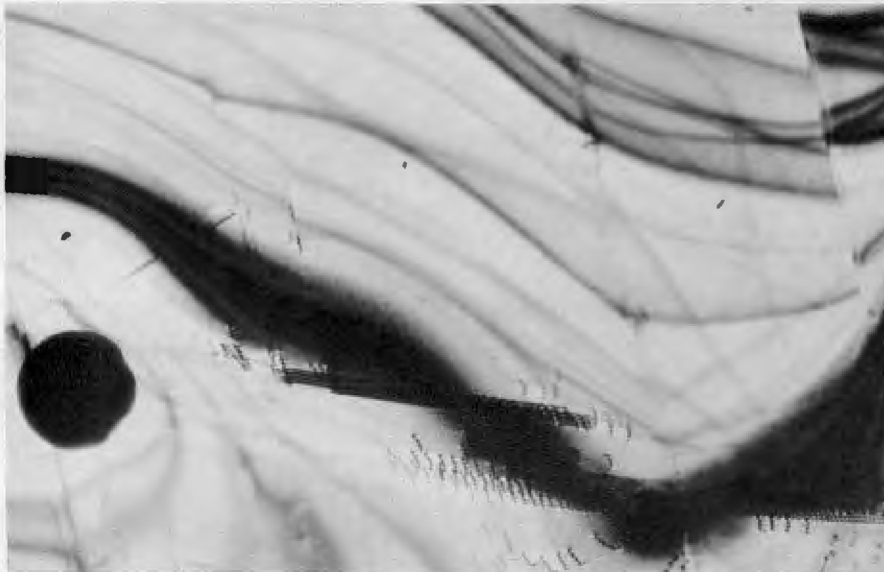

10b Fringes due to bent specimen, named "extinction contour". 20000:1

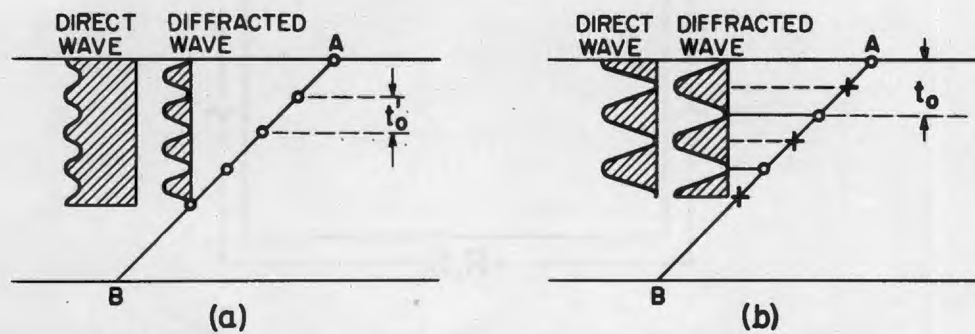

Fig. 11 Origin of diffraction fringes caused by a stacking fault.
(a) Spacing of fringes according to kinematical theory and
(b) due to the dynamical theory of electron diffraction (after Howie and Whelan (24)).

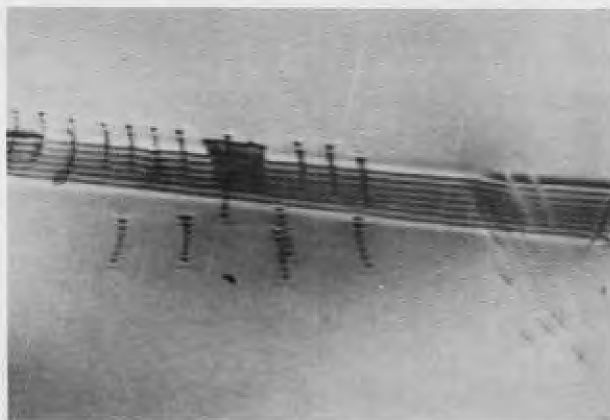

Fig. 12 Diffraction fringes due to
(a) a stacking fault, 40000:1; and (b) a grain or twin boundary, 40000:1

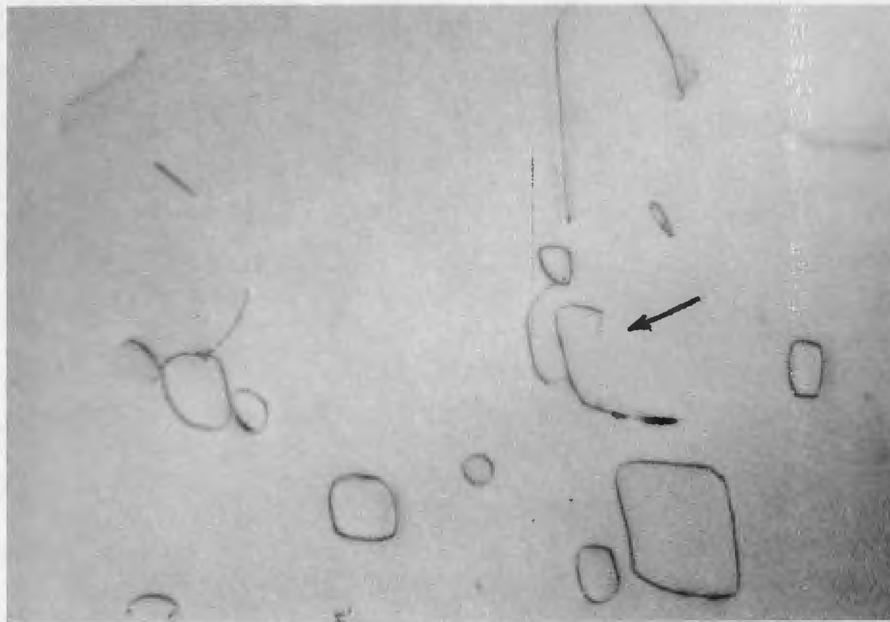

Fig. 13 Square-shaped dislocation loops in quenched and aged Al-0.5% Mg specimen. 40000:1
Micrograph by courtesy of I. G. Greenfield

Fig. 14 "Punched-out" loops in molybdenum single crystal. 40000:1
Micrograph by courtesy of H. Gaigher and A. Lawley